phys. stat. sol. (b) **235**, No. 2, 267–276 (2003) / **DOI** 10.1002/pssb.200301567

Specific features of the electronic structure of III–VI layered semiconductors: recent results on structural and optical measurements under pressure and electronic structure calculations

A. Segura[*,1], **F. J. Manjón**[1,4], **D. Errandonea**[1], **J. Pellicer-Porres**[1], **V. Muñoz**[1], **G. Tobias**[2], **P. Ordejón**[2], **E. Canadell**[2], **A. San Miguel**[3], and **D. Sánchez-Portal**[5]

[1] Institut de Ciència dels Materials, Universitat de València, Departamento de Física Aplicada, Ed. Investigació, 46100 Burjassot (València), Spain
[2] Institut de Ciència dels Materials de Barcelona, CSIC, Campus de la UAB, 08193 Bellaterra, Barcelona, Spain
[3] Physique des Matériaux, Université de Lyon I, 69622 Villeurbanne, France
[4] Departament de Física Aplicada, Universitat Politécnica de València, EPSA, 03801 Alcoi, Spain
[5] Centro Mixto CSIC-UPV/EHU and Donostia International Physics Center (DIPC), Apt. 1072, 20080 San Sebastian, Spain

Received 5 August 2002, revised 25 September 2002, accepted 25 September 2002
Published online 4 February 2003

PACS 61.10.Ht, 61.50.Ks, 64.70.Kb, 71.20.Nr, 78.40.Fy

In this paper we review some recent results on the electronic structure of III–VI layered semiconductors and its dependence under pressure, stressing the specific features that differentiate their behaviour from that of tetrahedrally coordinated semiconductors. We will focus on several unexpected results that have led to changes in the image that was currently accepted a few years ago. Intralayer bond angles change under pressure and the layer "thickness" remains virtually constant or increases. As a consequence, models based in intra- and inter-layer deformation potentials fail in explaining the low pressure nonlinearity of the band gap. Numerical-atomic-orbital/density-functional-theory electronic structure calculations allow for an interpretation of the evolution of the absorption edge under pressure. In particular, they show how the structure of the non-degenerated valence band maximum in InSe becomes more complex under pressure leading to a non-conventional direct-to-indirect crossover. The valence band maximum in InSe above 4 GPa exhibits a quite singular feature: a "ring-shaped" constant energy surface and, consequently, a density of states depending on energy as in 2D electronic systems.

1. Introduction The strongly anisotropic crystal structure of III–VI layered semiconductors (Fig. 1) gives rise to optical and mechanical anisotropies and non-linearities in the pressure dependence of some physical quantities. These effects were early identified [1] and extensively studied in the 80s and 90s [2–6]. Reports of X-ray experiments under pressure were not available until the end of the 80s and, unfortunately, they did not provide much information about the pressure dependence of the internal structure of the unit cell [7]. In that context, the evolution of the band structure under pressure was explained through a model based on intralayer and interlayer deformation potentials [2, 3]. This model was suggested by early empirical pseudopotential electronic structure calculations [8] and its main assump-

[*] Corresponding author; e-mail: alfredo.segura@uv.es

 0370-1972/03/23502-0267 $ 17.50+.50/0

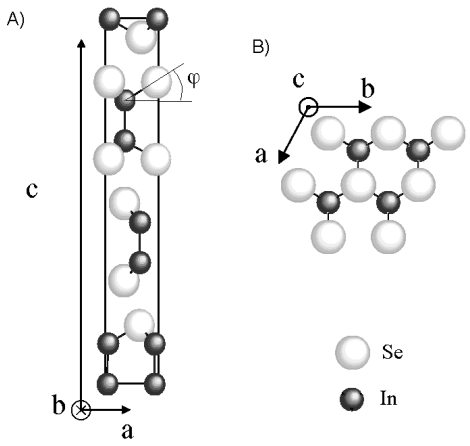

Fig. 1 Sketch of the crystal structure of InSe: A) projection in the (010) crystal plane, perpendicular the unit cell vector ***b***; B) projection in the (001) crystal plane plane, perpendicular to the unit cell vector ***c***.

tion was considering that all intralayer distances scald with the variation of the a parameter under pressure. From this assumption, and the pressure dependence of the c parameter, the change of interlayer distances under pressure could be modelled and the deformation potentials were obtained through a fit to the band gap pressure dependence.

X-ray absorption spectroscopy (XAS) experiments under pressure [9] yielded some unexpected results on the change of internal bond distances, showing that not all intralayer distances scale with a under pressure. This result changes the image that was currently accepted a few years ago and invalidates the main assumption of the two deformation potential model.

In this paper we review some recent results on the electronic structure of III–VI layered semiconductors and its dependence under pressure, stressing the specific features that differentiate their behaviour from that of tetrahedrally coordinated semiconductors. After a brief recall of experimental and calculation methods in Section 2, Section 3 will be devoted to the results of XAS experiments. Results of optical measurements under pressure will be presented in Section 4. Electronic structure calculations presented in Section 5 will be the base to discuss all these results and integrate them in a coherent view of the electronic structure of III–VI layered semiconductors.

2. Experimental and calculation methods The experimental details have been extensively described in Refs. [9–11]. A detailed description of the calculation method can be found in Ref. [11] (and references therein). The optical response was obtained using the first order time-dependent perturbation theory to calculate the dipolar transition matrix elements between occupied and unoccupied single-electron eigenstates, as implemented in Ref. [10]. The optical matrix elements were calculated including the corrections due to the non-locality of the pseudopotential [11].

3. Results of XAS experiments under pressure Figure 2 shows the evolution of the intralayer first neighbour Se–In distance, as obtained from XAS experiments under pressure [9]. This distance follows a monotonous compression up to 7.1 GPa, that can be accounted for by a Murnaghan-type equation of state:

$$d_{\mathrm{InSe}} = d_{\mathrm{InSe0}}\left(1+\frac{B_0'}{B_0}P\right)^{-\frac{1}{3B_0'}}, \tag{1}$$

where d_{InSe0} is the In–Se distance at ambient pressure, B_0 the local isothermal bulk modulus, and B_0' its pressure derivative. The data dispersion and the small pressure range do not allow for obtaining B_0 and B_0' simultaneously. We have fixed B_0' to a value of 5, resulting in a bulk modulus of B_0 = (116 ± 20) GPa. Similar evolution is found for GaSe and GaTe, for which the values of B_0 are (92 ± 6) GPa and (124 ± 6) GPa, respectively. On the other hand, from X-ray diffraction (XRD) experiments under pressure [7, 12,

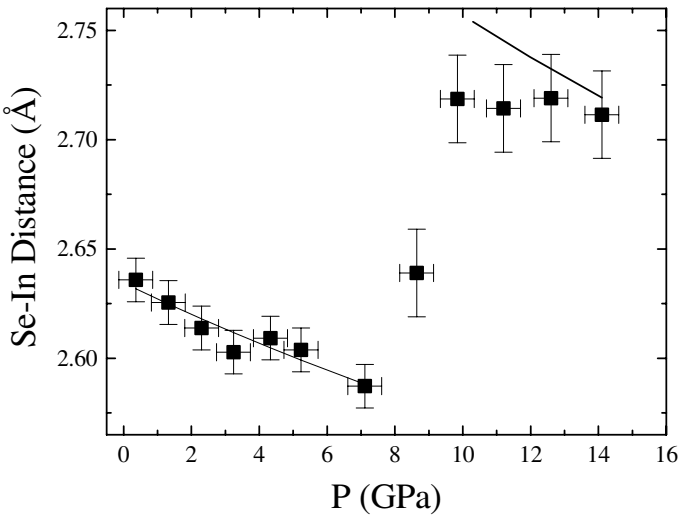

Fig. 2 Pressure dependence of the intralayer first neighbour In–Se distance, as obtained from EXAFS analysis.

13] it is possible to deduce the bulk modulus corresponding to the "a" parameter of the hexagonal cell, that turns out to be 44 GPa for InSe [7, 14] and (61 ± 4) GPa for GaSe [15], with B_0' fixed to 5. It is then clear that the In–Se (Ga–Se) bond-length and the a-axis do not shrink at the same rate. This implies that the angle φ between the In–Se bond and the layer plane (see Fig. 1) must change under pressure. As the trigonal axis defined by the In–In bond remains perpendicular to the layer under compression, the next equation follows:

$$\frac{a}{2} = d_{\mathrm{InSe}} \cos\varphi \cos 30\,. \tag{2}$$

The change of the angle under pressure can be so obtained and we find that φ grows from 28.7° ± 0.7° at ambient pressure to 31.4° ± 0.7° at 10 GPa.

On the hypothesis that the cation–cation bond compressibility is close to the cation–anion one, which has been proved in the case of GaS [16] and GaTe [17], it is possible to give the evolution of the whole

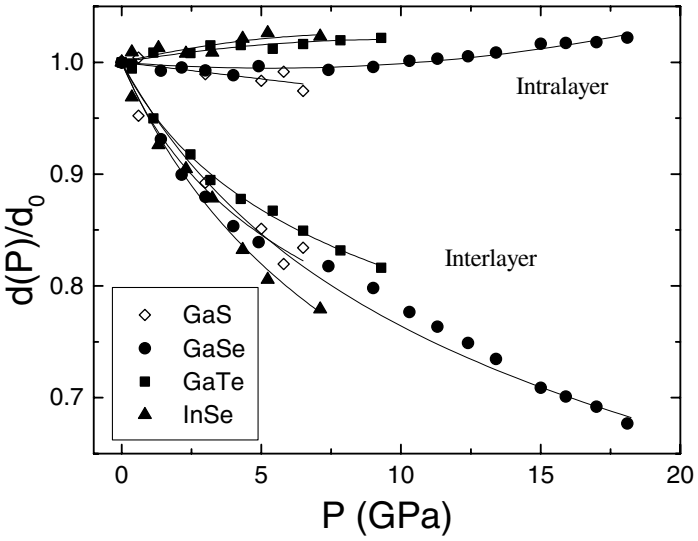

Fig. 3 Pressure evolution of interlayer and intralayer distances in III–VI semiconductors, as calculated through the model described in Section 3 (Eqs. (3) and (4)).

structure under pressure. In particular, it is possible to obtain the pressure dependence of intra- and interlayer distances between the anion planes:

$$d_{\text{intralayer}} = d_{\text{InIn}} + 2d_{\text{InSe}} \sin\varphi\,, \tag{3}$$

$$d_{\text{interlayer}} = \frac{c}{3} - d_{\text{intralayer}}\,. \tag{4}$$

The relative change of these distances, as calculated on the basis of the previous hypothesis is shown in Fig. 3, for GaS, GaSe, GaTe, and InSe. That pressure evolution clearly contradicts the hypothesis on which constant deformation potential models were based. With this pressure change of interlayer distances, no constant deformation potential model would account for the pressure evolution of the band gap. In fact, its low pressure non-linearity exhibits an exponential dependence on the interlayer distance. Being a consequence of interlayer van der Waals interactions, even sophisticated density-functional-theory (DFT) band structure calculations fail in accounting for that behaviour.

4. Pressure dependence of the absorption edge Figure 4 shows the evolution of the fundamental absorption edge of InSe, for a light polarization perpendicular to the *c*-axis, as a function of pressure. At low pressures the absorption edge shows a red-shift, reaching a minimum at 0.4 GPa (in GaSe that minimum occurs at about 1.3 GPa) [2, 3]. Above that pressure range, the fundamental edge shifts towards higher energies. The absorption intensity, which can be inferred from the exciton step-structure, also exhibits a minimum around 1.5 GPa and increases for higher pressures.

The step-like fundamental edge has been analyzed with the Elliot–Toyozawa model for the direct absorption including electron–hole interaction, in the analytical expression given by Goñi et al. [18]. A more detailed analysis of the absorption edge shows that this contribution is not enough to describe the change of the absorption edge under pressure: two quadratic contributions *with different pressure coefficients* yield a much better fit. We will refer to the quadratic edges of low and high onset energy as I_1 and I_2, respectively.

Figure 5 shows the pressure dependences of the direct and indirect edges in InSe and $In_{0.88}Ga_{0.12}Se$, as resulting from the fitting procedure. Both in InSe and $In_{1-x}Ga_xSe$, the three transitions show nonlinear pressure dependences at low pressures and almost a linear behavior above 2 GPa. A similar nonlinear behavior of the band gaps has also been previously observed in InSe [2, 4, 6], and also in GaSe [2, 3] and

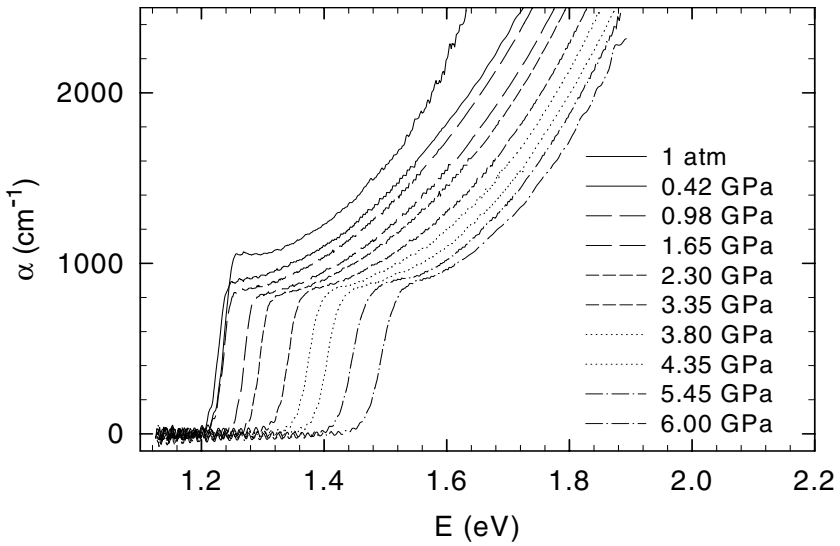

Fig. 4 Absorption edge of InSe at different pressures.

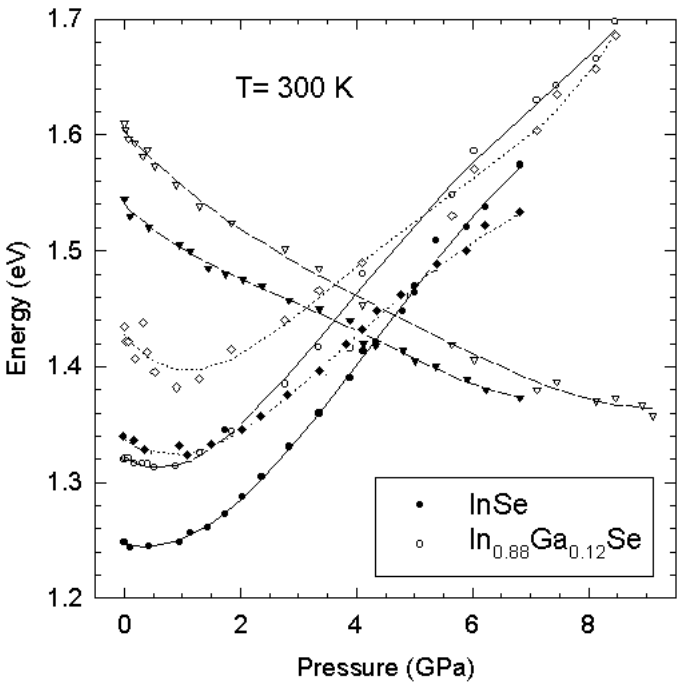

Fig. 5 Pressure dependence of electronic transitions in InSe (filled symbols) and $In_{0.88}Ga_{0.12}Se$ (hollow symbols). Circles, diamonds and triangles correspond to the direct gap at Z, I_1 indirect gap, and I_2 indirect gap, respectively.

GaTe [19]. In InSe, the linear pressure coefficients above 2 GPa are 62 meV/GPa, 42 meV/GPa, and –22 meV/GPa for the Z, I_1, and I_2 transitions, respectively. The energy differences between the I_1 and I_2 indirect edges with respect to the Z direct gap show an almost linear pressure dependence in the whole pressure range, with pressure coefficients of (–76 ± 10) meV/GPa and (–19 ± 5) meV/GPa for the I_2–Z and I_1–Z energy differences, respectively.

5. Band structure under pressure Figure 6 shows the evolution of the band structure in the region of the band gap for different pressures, as calculated through the numeric-atomic-orbital-density-functional theory (NAO-DFT) method in the H–Z–B path of the Brillouin zone (Bz). The assignment of the direct absorption edge to the valence band maximum (VBM) to conduction band minimum (CBM) transition at the Z point of the Bz seems the most natural and reasonable one.

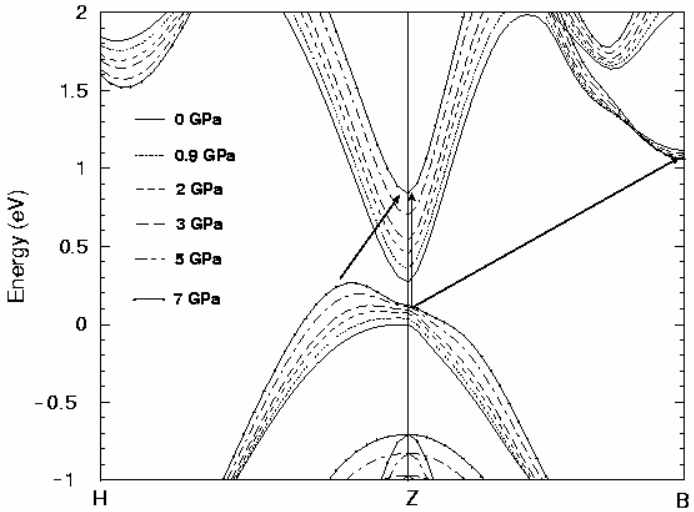

Fig. 6 NAO-DFT calculated band structure of InSe at different pressures in the energy region of the energy gap.

Let us now discuss the assignment of the quadratic absorption edges on the basis of electronic structure calculations. Two nonequivalent minima exist in the conduction band of InSe, at points A and B of the Bz, which are located above the absolute minimum at the Z point of the Bz at zero pressure. Under pressure, both minima shift down in energy, but the B minima remain lower in energy and shifts down with a higher pressure coefficient. Above 2 GPa, the pressure coefficients of the direct Z–Z, ZH to Z and Z to B transitions are 68 meV/GPa, 41 meV/GPa, and –13 meV/GPa, respectively. The calculated pressure coefficient of the energy difference between the Z to B indirect transition and the Z direct transition is –89 meV/GPa (average value from 0 to 7 GPa), which is very close to the experimental value of the Z–I_2 energy difference ((–76 ± 10) meV/GPa). From these results, the assignment of the I_2 indirect edge to a Z–B indirect transition seems quite well founded.

Regarding the I_1 edge, results of Fig. 6 give also the key for the assignment. This indirect edge would correspond to an indirect transition from the VBM that develops under pressure (both in the K–L and K–H directions) to the CBM at the Z point of the Bz. It must be remarked that in the β-InSe or the ε-InSe band structures calculated through empirical pseudopotential methods [8, 20], the absolute maximum of the valence band was found to be in the Γ–K direction. The first strong experimental evidence of this direct-to-indirect band gap crossover in InSe was given by the pressure behavior of the exciton width at low temperature, but it was interpreted on the basis of the I_2 direct-to-indirect cross-over [7]. The calculated pressure coefficient of the energy difference between the ZH to Z indirect transition and the Z direct transition, as calculated through the NAO-DFT method is –20 meV/GPa (average value from 0 to 7 GPa). This result is in good agreement with the experimental value of the I_1–Z energy difference ((–19 ± 5) meV/GPa) and supports the assignment of the I_1 indirect edge to the ZH to Z transition.

A more detailed calculation of the constant energy surface of this new VBM reveals that it has quasi-cylindrical symmetry with respect to the *c*-axis, in such a way that the constant energy surfaces are ring-shaped as shown in Fig. 7. At pressures larger than 4 GPa, this would be the absolute valence band maximum. If one assumes cylindrical symmetry, and a circular cross section of the ring with a plane containing the k_z axis (*c*-axis direction), the density of states corresponding to this VBM would be:

$$g_V(E) = 0\,; \qquad E > E_V\,,$$

$$g_V(E) = \frac{m^*_{V2}}{\pi\hbar^2}\,k_M\,; \qquad E < E_V\,, \tag{5}$$

where k_M is the radius of the ring central circumference and m^*_{V2} is the effective mass.

Hall effect measurements in p type InSe confirm the existence of a change in the VBM under pressure. The large increase of both the hole concentration and the hole mobility under pressure [21] can be understood on the basis of a corresponding large increase of the density of states and a decrease of the effective mass in the VBM. These apparently contradictory conditions can be fulfilled in the ring shaped VBM, with a density of states given by Eq. (5).

Let us try to understand the origin of this specific feature of the InSe VBM, in the framework of the $\boldsymbol{k}\cdot\boldsymbol{p}$ model. The reciprocal effective masses at the Z valence band maximum are given by [22]

$$\left[\frac{m_0}{m^*_{\nu Z}}\right]_{\perp} = 1+\frac{2}{m_0}\sum_n \frac{\left|\langle \nu Z_1|\ P_\perp\ |n\rangle\right|^2}{E_{\nu Z}-E_n}\,, \tag{6}$$

and

$$\left[\frac{m_0}{m^*_{\nu Z}}\right]_{\parallel} = 1+\frac{2}{m_0}\sum_n \frac{\left|\langle \nu Z_1|\ P_\parallel\ |n\rangle\right|^2}{E_{\nu Z}-E_n} \tag{7}$$

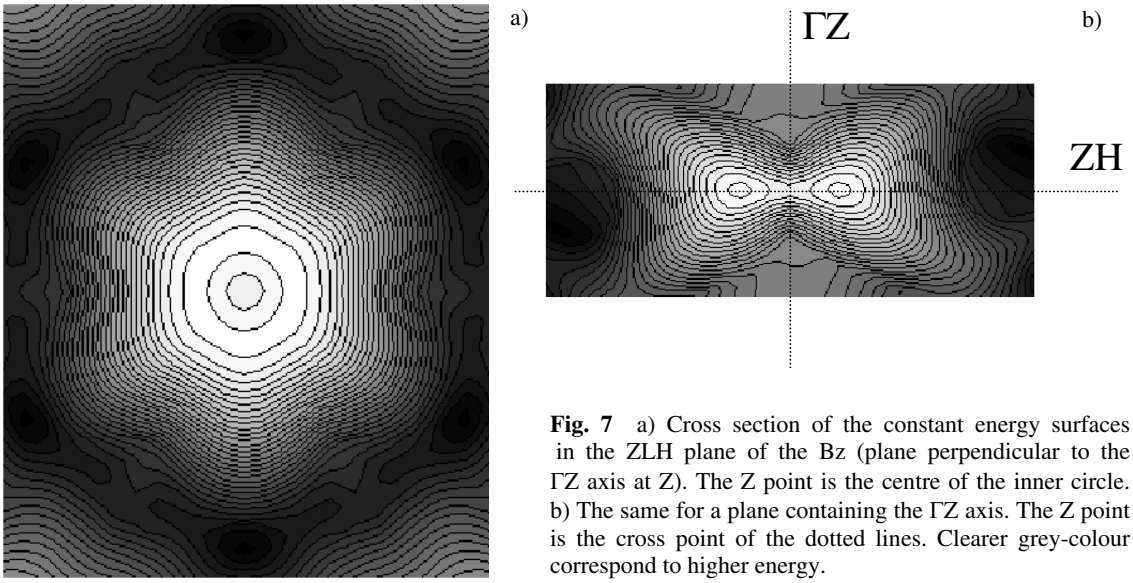

Fig. 7 a) Cross section of the constant energy surfaces in the ZLH plane of the Bz (plane perpendicular to the ΓZ axis at Z). The Z point is the centre of the inner circle. b) The same for a plane containing the ΓZ axis. The Z point is the cross point of the dotted lines. Clearer grey-colour correspond to higher energy.

for the electron wave-vector perpendicular and parallel to the *c*-axis, respectively. $\langle v\mathrm{Z}_1 \mid P_{\perp,\parallel} \mid n\rangle$ stands for the dipolar matrix element between the valence band maximum and other extrema at the Z point for light polarization parallel and perpendicular to the *c*-axis. At the Z point the uppermost valence band has predominant Se p_z character and the lowermost conduction band has predominant In *s* character. Both electronic states belong to the Z_1 representation of the C_{3v} point group and the transition between them (i.e., the fundamental transition) is fully allowed only for light polarization parallel to the *c*-axis. The transition between them is forbidden for a polarization perpendicular to the *c*-axis, as illustrated in Fig. 8, that shows the calculated imaginary part of the dielectric function of InSe for polarizations parallel and perpendicular to the *c*-axis.

As the matrix element with the conduction band for light polarization parallel to the *c*-axis is very large [23], Eq. (7) leads to a negative and small effective mass, which is coherent with the large dispersion exhibited by the valence band in the Γ–Z direction:

$$\left[\frac{m_0}{m_{v\,\mathrm{Z}}}\right]_{\parallel} \approx -\frac{2}{m_0}\,\frac{\left|\langle v\mathrm{Z}_1 \left| P_{\parallel} \right| c\mathrm{Z}_1\rangle\right|^2}{E_{\mathrm{g}}}\,. \tag{8}$$

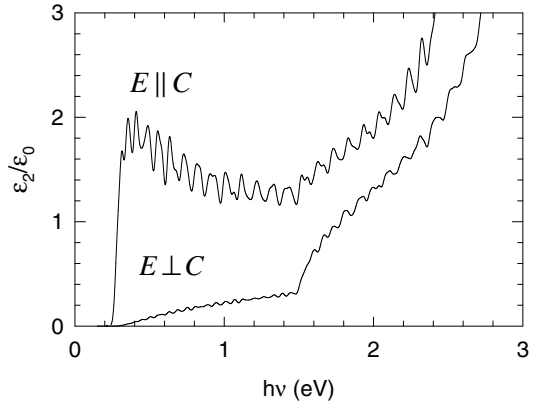

Fig. 8 Imaginary part of the dielectric function of InSe for light polarization perpendicular and parallel to the *c*-axis, as calculated by the method described in Section 2.

However, for light polarization perpendicular to the *c*-axis, allowed transitions to the Z_1 bands with large matrix elements are: i) those from Z_3 valence bands (with Se p_x–p_y character) lying 1 to 1.5 eV below the uppermost valence band and ii) those from Z_3 conduction bands (with In p_x–p_y character) lying 4 to 5 eV above the uppermost valence band [24]. With these considerations, Eq. (6) leads to

$$\left[\frac{m_0}{m_{vZ}}\right]_{\perp} = 1 + \frac{\left|\langle vZ_1 \left| P_{\perp} \right| vZ_3 \rangle\right|^2}{E_{vZ_1} - E_{vZ_3}} + \frac{\left|\langle vZ_1 \left| P_{\perp} \right| cZ_3 \rangle\right|^2}{E_{vZ_1} - E_{cZ_3}} . \tag{9}$$

As the second term in the right hand side (r.h.s.) of Eq. (9) is positive and the third one is negative, they compensate each other leading to a large value of the hole effective mass in the layer plane. This large value is coherent with the low dispersion of the valence band in directions Z–L and Z–H, near to the Z point. Consequently, the hole effective mass turns out to have an "anomalous" anisotropy. An experimental estimation of the hole effective mass tensor, obtained from the shallow acceptor ionization energy [25], yielded $m_{h\perp}/m_{hII} = 3.5$, which confirms this anomalous anisotropy.

The previous discussion suggests an interpretation of the emergence of the ring shaped maximum: NAO–DFT band structure calculations show that the energy difference between Z_3 In p_x–p_y conduction bands and the uppermost valence band ($(E_{vZ_1} - E_{cZ_3})$ in Eq. (9)) increases under pressure, whereas the energy difference between the uppermost valence band and the Z_3 Se p_x–p_y valence bands ($(E_{vZ_1} - E_{vZ_3})$ in Eq. (9)) decreases under pressure (Fig. 6). This means that the negative term in Eq. (9) ($\boldsymbol{k} \cdot \boldsymbol{p}$ interaction with Z_3 conduction bands) decreases in the absolute value and the positive term ($\boldsymbol{k} \cdot \boldsymbol{p}$ interaction with Z_3 valence bands) increases under pressure, resulting in a positive curvature for the uppermost valence band at Z above a given pressure.

In a more realistic model, one has to take into account two more interactions: (i) on the one side spin–orbit interaction mixes p_z and p_x–p_y states belonging to the C_{3v} double group Z_6 representation (J = 1/2), and (ii) on the other side, even in the absence of spin–orbit interaction, p_z and p_x–p_y states belong to a different representation only in the Γ–Z line of the Brillouin zone. Away from it they mix and this is the reason why the dielectric function slowly grows with the photon energy above the fundamental gap (Fig. 8). The photon energy dependence of the matrix element on the photon energy can give an estimation of the p_x–p_y Z_3 component in the states near to the VBM. From that dependence we find that the matrix element depends linearly on $(h\nu - E_g)$, which indicates a dependence on the square of the electron wavevector.

Then, the wave function of states near to the valence band maximum in the k_xk_y plane can be written as

$$|\, vZ, \boldsymbol{k}_{\perp}\rangle = |vZ_1\rangle + A\,|vZ_3\rangle + Bk_{\perp}^2\,|vZ_3\rangle\,, \tag{10}$$

where A and B are constants related to spin orbit interaction and p_z–(p_x–p_y) mixing away from the Γ–Z axis, respectively. Their matrix element with the lowest conduction band would be

$$\langle vZ, \boldsymbol{k}_{\perp}|\; P_{\perp}\; | cZ\rangle = A\langle vZ_3|\; P_{\perp}\; | cZ_1\rangle + Bk_{\perp}^2\langle vZ_3|\; P_{\perp}\; | cZ_1\rangle \tag{11}$$

Then, a new term should be added to Eq. (9), in order to give the dependence of the effective mass on $\boldsymbol{k}_{\perp}$

$$\left[\frac{m_0}{m_{vZ}}\right]_{\perp}(\boldsymbol{k}_{\perp}) = \left[\frac{m_0}{m_{vZ}}\right]_{\perp}(0) - (A + Bk_{\perp}^2)^2\,\frac{\left|\langle vZ_3|\; P_{\perp}\; | cZ_1\rangle\right|^2}{E_g}\,, \tag{12}$$

where the first term includes all terms in the r.h.s. of Eq. (9). Then, even if at a given pressure the first term is positive and the valence near to Z disperses "upwards" for small values of $\boldsymbol{k}_{\perp}$, the second term

will dominate at a given value of $\boldsymbol{k}_\perp$ and the effective mass will become negative, which results in a new VBM away from the *c*-axis, with quasi-cylindrical symmetry.

6. Spin–orbit splitting of Z_3 valence bands The absorption spectra of InSe and GaSe exhibit only two transitions at 1.15 and 1.5 eV above the fundamental one [6, 26]. This contrasts with the fact that there are two pairs of valence bands with Se p_x–p_y character (belonging to the Z_3 representation), that would split in four nondegenerate bands due to spin−orbit interaction. The calculated dielectric function shown in Fig. 8 gives us the key to understand this apparent contradiction. The sketch of Fig. 9 compares the dielectric function to the band structure, evidencing that the lowest pair of p_x–p_y bands does not give any contribution to the dielectric function, even if it would be allowed by selection rules.

From an LCAO point of view, the couple of doubly degenerate Se p_x−p_y states at Z can be seen as symmetric and antisymmetric combinations of the states of the half layers. If we neglect the normalization coefficient, they can be described with wave functions $|\nu_2\rangle = |\nu_\alpha\rangle + |\nu_\beta\rangle$ and $|\nu_3\rangle = |\nu_\alpha\rangle - |\nu_\beta\rangle$, where α and β stand for each half-layer. As the energy separation between these states is relatively low, it is reasonable to assume that the coefficients in the linear combinations are close to 1 and −1. The matrix elements of the transitions from these states to the conduction band for light polarization perpendicular to the *c*-axis would be:

$$\begin{aligned} P_{V2\to c} &= \langle \nu_2|\, P_\perp\, |c\rangle = \langle \nu_\alpha|\, P_\perp\, |c\rangle \;+\; \langle \nu_\beta|\, P_\perp\, |c\rangle \\ P_{V3\to c} &= \langle \nu_2|\, P_\perp\, |c\rangle = \langle \nu_\alpha|\, P_\perp\, |c\rangle \;-\; \langle \nu_\beta|\, P_\perp\, |c\rangle\,. \end{aligned} \tag{13}$$

As the states in the half layers are identical, one of the matrix elements will be almost zero and the other will be very large. In presence of the spin–orbit interaction each couple of Z_3 states split in Z_6 (J = 1/2) and Z_4–Z_5 (J = 3/2) states. Spin–orbit split states corresponding to the initial state of E_{g2} transition in Fig. 9 give rise to the two observed intense transitions in InSe and GaSe and the other two are not observed due to the low value of the matrix element. This discussion is coherent with previous assignments of the energy difference between these transitions to the spin−orbit interaction, based in its insensitivity to pressure [6] or in an extension of the Hopfield's quasi-cubic model [26, 27].

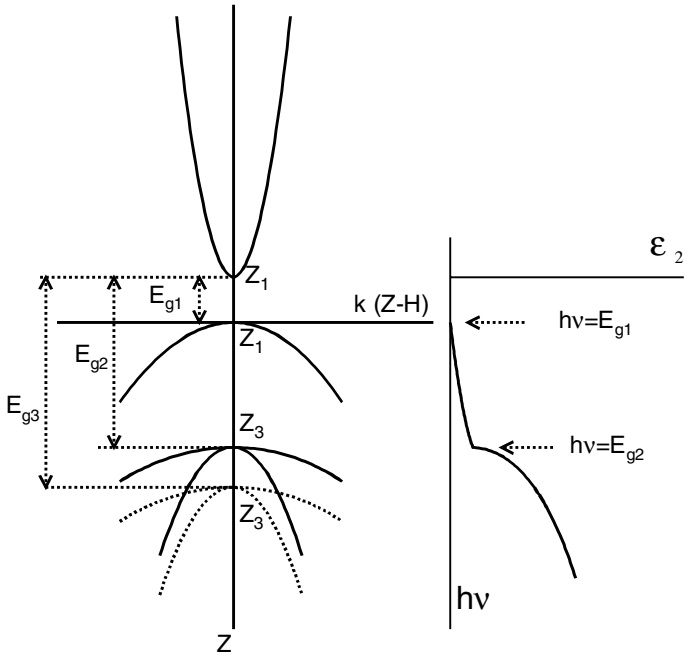

Fig. 9 Sketch of the InSe band structure compared to the dielectric function for light polarization perpendicular to the *c*-axis.

6. Conclusion and open problems This paper illustrates how optical measurements under pressure, in combination with DFT calculations, are a very efficient tool for understanding a semiconductor electronic structure, even in materials with low symmetry and high anisotropy as III–VI layered materials. In spite of the amount of new results provided by these techniques, there are many open problems in the subject. Probably the most difficult one is giving quantitative theoretical account of the nonlinearity in the pressure dependence of the band gap. Even if we know that van der Waals interlayer interactions are at the origin of that behaviour, the problem remains open because DFT calculations fail in describing correctly this kind of interactions, as they depend on density fluctuation correlations, rather than on the local electron density or its gradient.

References

[1] J. M. Besson, K. P. Jain, and A. Khun, Proc. 12th Internat. Conf. Phys. Semicond., edited by M. H. Pilkuhn (B. G. Teubner Verlagsgesellschaft, Stuttgart, 1974), p. 987.
[2] N. Kuroda, O. Ueno, and Y. Nishina, J. Phys. Soc. Jpn. **55**, 581 (1986).
[3] M. Gauthier, A. Polian, J. M. Besson, and A. Chevy, Phys. Rev. B **40**, 3837 (1989).
[4] A. R. Goñi, A. Cantarero, U. Schwarz, K. Syassen, and A. Chevy, Phys. Rev. B **45**, 4221 (1992).
[5] D. Errandonea, F. J. Manjón, J. Pellicer, A. Segura, and V. Muñoz, phys. stat. sol. (b) **211**, 33 (1999).
[6] C. Ulrich, D. Olguin, A. Cantarero, A. R. Goñi, K. Syassen, and A. Chevy, phys. stat. sol. (b) **221**, 777 (2000).
[7] U. Schwarz, A. R. Goñi, K. Syassen, A. Cantarero, and A. Chevy, High Press. Res. **8**, 396 (1991).
[8] A. Bourdon, A. Chevy, and J. M. Besson, in: Physics of Semiconductors 1978, Proc. 14th Internat. Conf. Phys. Semicond., edited by B. L. H. Wilson, IOP Conf. Proc. **43** (Institute of Physics and Physical Society, London, 1979), p. 1371.
[9] J. Pellicer-Porres, A. Segura, V. Muñoz, and A. San Miguel, Phys. Rev. B **60**, 3757 (1999).
[10] J. M. Soler, E. Artacho, J. D. Gale, A. Garcia, J. Junquera, P. Ordejon, and D. Sanchez-Portal, J. Phys., Condens. Matter **14**, 2745 (2002).
[11] A. J. Read and R. J. Needs, Phys. Rev. B **44**, 13071 (1991).
[12] D. Errandonea, A. Segura, V. Muñoz, and A. Chevy, Phys. Rev. B **60**, 15866-74 (1999).
[13] F. J. Manjón, D. Errandonea, A. Segura, V. Muñoz, G. Tobías, P. Ordejón, and E. Canadell, Phys. Rev. B **63**, 125330 (2001).
[14] D. Olguin, A. Cantarero, C. Ulrich, and K. Syassem, phys. stat. sol. (b) **235**, 456 (2003) (this issue).
[15] M. Takumi, A. Hirata, T. Ueda, Y. Koshio, H. Nishimura, and K. Nagata, phys. stat. sol. (b) **223**, 423 (2001).
[16] H. d'Amour, W. B. Holzapfel, A. Polian, and A. Chevy, Solid State Commun. **44**, 853 (1982).
[17] J. Pellicer-Porres, A. Segura, and A. S. M. y V. Muñoz, Phys. Rev. B **61**, 125 (2000).
[18] A. R. Goñi, A. Cantarero, K. Syassen, and M. Cardona, Phys. Rev. B **41**, 10111 (1990).
[19] J. Pellicer-Porres, F. J. Manjón, A. Segura, V. Muñoz, C. Power, and J. González, Phys. Rev. B **60**, 8871 (1999).
[20] Y. Depeursinge, Il Nuovo Cimento **64B**, 111 (1981).
[21] D. Errandonea, to be published.
[22] E. O. Kane, J. Phys. Chem. Solids **1**, 249 (1957).
[23] N. Kuroda and I. Nishina, Physica B **105**, 30 (1980).
[24] N. Piccioli, R. Le Toullec, F. Bertrand, and J. C. Chervin, J. Phys. **42**, 1129 (1981).
[25] Ch. Ferrer-Roca, A. Segura, M. V. Andres, J. Pellicer, and V. Muñoz, Phys. Rev. B **55**, 6981 (1997).
[26] N. Kuroda, I. Munakata, and Y. Nishina, Solid State Commun. **33**, 687 (1980).
[27] J. J. Hopfield, J. Phys. Chem. Solids **15**, 97 (1960).